



Cite this: *Analyst*, 2016, **141**, 1734

Quantitative electrochemical metalloimmunoassay for TFF3 in urine using a paper analytical device†

Paul R. DeGregory,^a Yi-Ju Tsai,^a Karen Scida,^{‡a} Ian Richards^b and Richard M. Crooks^{*a}

We report a paper-based assay platform for the detection of the kidney disease marker Trefoil Factor 3 (TFF3) in human urine. The sensor is based on a quantitative metalloimmunoassay that can determine TFF3 concentrations *via* electrochemical detection of environmentally stable silver nanoparticle (AgNP) labels attached to magnetic microbeads *via* a TFF3 immunosandwich. The paper electroanalytical device incorporates two preconcentration steps that make it possible to detect concentrations of TFF3 in human urine at the low end of the target TFF3 concentration range (0.03–7.0 $\mu\text{g mL}^{-1}$). Importantly, the paper device provides a level of accuracy for TFF3 determination in human urine equivalent to that of a commercial kit. The paper sensor has a dynamic range of ~ 2.5 orders of magnitude, only requires a simple, one-step incubation protocol, and is fast, requiring only 10 min to complete. The cost of the materials at the prototypic laboratory scale, excluding reagents, is just US\$0.42.

Received 17th November 2015,
Accepted 18th January 2016

DOI: 10.1039/c5an02386f

www.rsc.org/analyst

Introduction

Here we report an electrochemical metalloimmunoassay for Trefoil Factor 3 (TFF3) that is compatible with an inexpensive paper-based electrochemical detection platform and effective for detection in human and artificial urine. TFF3 is one of three proteins expressed in bodily tissues, most notably in the gastrointestinal mucosa, that share the trefoil motif. This motif is a 40-amino acid domain containing 6 cysteine residues that form 3 disulfide bonds to create a three-leafed structure.¹ Although the function of TFF3 has not been fully determined, it has been suggested that TFF3 (and other secretory TFF peptides) helps to repair mucosal epithelial

injury *via* the formation of mucous barriers, anti-apoptotic and pro-angiogenic effects, restitution, and modulation of immune responsiveness, inflammatory processes, and differentiation.² The motivation for elucidating the usefulness of TFF3 in diagnostics stems from an unmet need for more sensitive and specific biomarkers indicative of renal health.^{3–5} The Predictive Safety Testing Consortium Nephrotoxicity Working Group laid out the rationale for improved renal biomarkers as follows: “given the societal cost of nephrotoxicity and the insensitivity of current methods to detect it, sensitive methods for prediction of toxicity in preclinical studies and identification of injury in humans are extremely important for patient safety in clinical practice and in all stages of the drug development process”.³ Blood urea nitrogen (BUN) and serum creatinine (SCr) have served as the standards for preclinical and clinical renal monitoring.^{3,5–7} However, these tests have often been found to lack the specificity and sensitivity required to assess whether the illness originates from kidney damage,^{3,5,7} and lack the diagnostic power to support the identification of the condition before severe illness manifests.^{3,5–7}

Several new renal biomarkers have recently been reported and found to be better indicators of renal health status and also to be more sensitive indicators of changes in renal function than their predecessors. For example, the urinary TFF3 level has shown promise as a biomarker for chronic kidney disease (CKD), which affects roughly 11% of the US population,⁸ and acute kidney injury (AKI), which is a risk factor for cardiovascular disease⁹ and develops in 30–50% of intensive care unit patients.¹⁰ Urinary TFF3 levels have been shown to

^aDepartment of Chemistry and the Center for Nano- and Molecular Science and Technology, The University of Texas at Austin, 105 E. 24th St., Stop A5300, Austin, TX 78712-1224, USA. E-mail: crooks@cm.utexas.edu; Tel: +1512-475-8674

^bInteractives Executive Excellence LLC, 201 N. Weston Lane, Austin, Texas 78733, USA

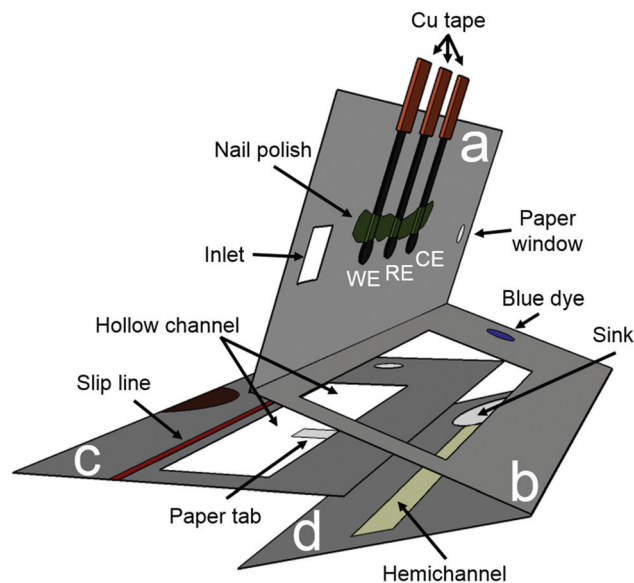
† Electronic supplementary information (ESI) available: Artificial urine preparation, collection of urine samples, M μ B/spAb conjugate and AgNP/2 $^{\circ}$ mpAb/mpAb conjugate preparation, AgNP/anti-TFF3 antibody screening for TFF3 activity, a list of anti-TFF3 antibodies screened for use as mpAb, plots of absorbance *vs.* M μ B/spAb volume and AgNP/2 $^{\circ}$ mpAb/mpAb concentration for assay optimization, plots of absorbance *vs.* TFF3 concentration for partially optimized and optimized conditions, a table showing the unspiked TFF3 concentrations in human urine samples, the TFF3 dose–response curve generated using the R & D Systems ELISA kit, a photograph of the assembled oSlip device, and a plot of absorbance *vs.* incubation time for the one-step incubation are provided. See DOI: 10.1039/c5an02386f

‡ Current address: 3M Center, Saint Paul, MN 55144.

increase in patients with CKD^{6,11,12} and were markedly reduced in urinary rat models with AKI induced *via* cisplatin and other pharmaceutical compounds.⁷ While trends in urinary TFF3 levels have been observed for certain renal ailments, there are currently no standard clinically relevant urinary TFF3 ranges for healthy or diseased individuals. The Nephrotoxicity Working Group of the Predictive Safety Testing Consortium is currently evaluating the expanded clinical utility of several qualified biomarkers, including TFF3, in human clinical research. However, previously published data have reported TFF3 concentrations in the urine of normal and diseased individuals to span the range between 0.03–7.0 $\mu\text{g mL}^{-1}$.^{6,12,13} Accordingly, and while acknowledging the evaluation status of TFF3 in the Predictive Safety Testing Consortium qualification process, we will refer hereafter to this as our “target range” so that we have a reasonable benchmark to compare to the results of our assay. Reports on existing TFF3 assays are available,^{1,14,15} but, to the best of our knowledge, an inexpensive, portable, point-of-care (PoC) test for TFF3, which could provide for improved patient monitoring and more reliable toxicological information during drug development, does not exist at the present time.

Low-cost, mass-produced PoC biosensors provide access to diagnostic and health monitoring technologies in resource-limited regions,¹⁶ benefit developed areas by enabling more convenient healthcare monitoring for individuals,^{17,18} increase drug development efficiency,^{19–23} and ease the workload on strained healthcare systems.²⁴ Paper analytical devices (PADs) show promise for serving as inexpensive, PoC biosensors and have experienced a surge in interest after Whitesides reported on a simple fabrication method for PADs in 2007.²⁵ This development was followed by a rapid acceleration in the advancement of PAD hardware,^{26–39} accompanied by expanding test sophistication whereby multistep immunoassays,^{40–44} oligonucleotide capture,^{45–50} conformational change at the detection site,^{51–53} and isothermal nucleic acid amplification,^{54,55} have all been demonstrated. A number of recent reviews of paper-based devices are available that discuss fabrication, device assembly, sensing schemes, detection methods, applications, and data readout.^{56–59}

We recently reported a 3D PAD design that is easily fabricated using the principles of origami (Japanese paper folding).⁶⁰ We call this device an *o*Slip to signify origami fabrication and the presence of a slip layer. In the present study we adapted this basic form factor to a TFF3 assay using urine as the matrix. The device design is shown in Scheme 1 and discussed in more detail later. The dynamic range of the *o*Slip-based TFF3 assay spans 2.5 orders of magnitude and overlaps most of the target TFF3 concentration range (0.03–7.0 $\mu\text{g mL}^{-1}$).^{6,12,13} Importantly, the *o*Slip assay and a commercial TFF3 enzyme-linked immunosorbent assay (ELISA) kit were found to agree within a relative error of 15% when analyzing samples of TFF3 spiked into artificial and human urine. The total *o*Slip assay time is <10 min and the cost of the materials at the lab scale, and excluding the cost of reagents, is ~US \$0.42.



Scheme 1

Experimental section

Chemicals and materials

Recombinant human TFF3 (13.2 kDa, MBS144182) was obtained from MyBioSource (San Diego, CA). Monoclonal mouse anti-human TFF3 solid-phase Ab (spAb) (MAB4407) was obtained from R & D Systems (Minneapolis, MN). Monoclonal rabbit anti-human TFF3 mobile-phase antibody (mpAb) (ab108599) was obtained from Abcam (Cambridge, MA). Biotinylated goat anti-rabbit secondary mobile-phase antibody (2° mpAb, 43R-1480) was obtained from Fitzgerald (North Acton, MA). Streptavidin-conjugated horseradish peroxidase (SA/HRP, N100) and 1-Step Ultra TMB-ELISA Substrate Solution (34028) were obtained from Thermo Scientific (Grand Island, NY).

Erioglaucine disodium salt (blue dye) was obtained from Acros Organics (Pittsburgh, PA). H_2SO_4 , 95.0–98.0 wt%, phosphate-buffered saline (PBS) (10× powder concentrate), NaOH, NaCl, $(\text{NH}_4)_2\text{SO}_4$, citric acid monohydrate, urea, CuCl_2 , MgSO_4 , Na_2SO_4 , KH_2PO_4 , K_2HPO_4 , NH_4Cl , NaHCO_3 , and HCl were obtained from Fisher Scientific (Pittsburgh, PA). Boric acid, ACS grade, was obtained from EM Science (Gibbstown, NJ). KMnO_4 and casein sodium salt from bovine milk (casein) were purchased from Sigma-Aldrich (St. Louis, MO). All solutions were prepared using deionized (DI) water (18.2 M Ω cm, Milli-Q Gradient System, Millipore, Bedford, MA).

Whatman grade 1 chromatography paper (20 cm × 20 cm × 180 μm thick) was from Fisher Scientific. Citrate-capped silver nanoparticles (AgNPs), nominally 20 nm in diameter (0.02 mg mL^{-1} in aqueous 2 mM citrate solution, pH 8), were obtained from nanoComposix (San Diego, CA). Magnetic microbeads (M μ Bs) having a diameter of 2.8 μm (Dynabeads M-270 Epoxy) were obtained from Life Technologies (Grand Island, NY). A 2 in × 1/2 in × 1/8 in thick neodymium rectangular magnet

(N40) was purchased from K & J Magnetics (Pipersville, PA) and used to separate and wash the M μ Bs during conjugation and some assays. A 1/16 in diameter \times 1/4 in long neodymium cylindrical magnet (N48) was acquired from Apex Magnets (Petersburg, WV) and used for *o*Slip experiments. Acrylic plates (0.6 cm thick), used to compress the *o*Slip, were obtained from Evonik Industries (AcryliteFF).

Costar 9017 medium binding microtiter plates were obtained from Corning (Corning, NY). Clear nail polish was purchased from Electron Microscopy Sciences (Hatfield, PA). Cu tape was obtained from 3M (Saint Paul, MN). Conductive carbon paste (CI-2042) was purchased from Engineered Conductive Materials (Delaware, OH).

Instrumentation

All electrochemical measurements were performed at 23 ± 2 °C using a potentiostat (Model 650C or 700E, CH Instruments, Austin TX). A conventional poly(tetrafluoroethylene) (Teflon) cell was used for some electrochemical measurements. A 1.0 mm-diameter glassy carbon working electrode (GCE), Ag/AgCl reference electrode ([KCl] = 1.0 M), and Pt wire counter electrode (CH Instruments) were used for electrochemical measurements carried out in the conventional cell.

Absorbance readings were obtained using a Synergy H4 Hybrid Multi-Mode Microplate Reader from BioTek (Winooski, VT). A Sorvall Legend Micro 21R Centrifuge from Thermo Scientific was used for washing and separation during AgNP conjugation. A Mini Vortexer 945300 from VWR International (Radnor, PA) was used to briefly mix solutions while a BioShake iQ from QUANTIFOIL Instruments GmbH (Germany) was used for assay incubations and AgNP and M μ B conjugate preparation. A VP 771HH-R handheld magnetic separator was obtained from V & P Scientific (San Diego, CA) and used to decant microtiter plates while retaining the M μ Bs. An Epilog (Golden, CO) laser engraving system (Zing 16) was used to cut stencils, hollow channels, and the acrylic holder for the *o*Slips. A Xerox (Norwalk, CT) ColorQube 8570DN inkjet printer was used for wax printing.

*o*Slip fabrication

The fabrication and operation of the *o*Slip have been described in detail previously.⁶⁰ Briefly, *o*Slip patterns were designed using Adobe Illustrator CS6 (version 16.0.0) and then wax printed on Whatman grade 1 chromatography paper using black wax for all patterns except for the hemichannel, which was printed using 60% yellow wax. The print-outs were heated at 130 °C for 30 s to melt the wax through the paper. The hollow channels were fabricated by cutting out a section of the paper with the laser engraving system. Individual paper devices were also cut from the paper sheets using the laser engraving system. Carbon ink was heated to 65 °C for 1 h, cooled to 4 °C, and then used to stencil print electrodes onto the *o*Slips. Stencil patterns were designed using Adobe Illustrator and cut into plastic transparency sheets using the laser engraving system. The printed electrodes were allowed to dry overnight at 23 ± 2 °C.

The next day, Cu tape was attached to the carbon ink contact pads and then a strip of nail polish was painted over a portion of the carbon ink bands that connect the electrode surfaces to the contact pads where Cu tape is fixed (Scheme 1). 4 μ L of blue dye were pipetted onto the paper circle depicted in Scheme 1, and then the nail polish and dye were dried for 30 min. A strip of Whatman 1 chromatography paper was placed over the 3 electrode surfaces and wet with DI water to increase the hydrophilicity of the carbon ink electrodes prior to use. After drying, the *o*Slips were folded as depicted in Scheme 1 and were ready for use.

Electrochemical detection

Electrochemical detection was carried out using anodic stripping voltammetry (ASV) both in the conventional cell and the *o*Slips. For detection in the conventional cell, a Ag deposition potential of -0.30 V (vs. Ag/AgCl) was applied for 200 s, followed by a 10 s quiet time at -0.10 V, and then a linear voltammetric sweep from -0.10 V to 0.40 V at 0.050 V s⁻¹. For detection on the *o*Slips, a similar procedure was followed, except the deposition potential was -0.60 V (vs. carbon quasi-reference electrode, cQRE) and the linear sweep was from -0.50 V to 0.20 V. Data were processed using OriginPro 8 software and data points were treated according to Dixon's *Q* test. Error bars represent one standard deviation from mean values.

Procedures for stepwise and one-step assays

The procedures for preparing the M μ B/spAb and AgNP/2°mpAb/mpAb conjugates are provided in the ESI.† Both the stepwise and one-step assays were carried out in medium-binding microtiter plates blocked with 1 wt% casein in 100 mM borate (pH 7.5, overnight, 4 °C). For the stepwise assays, the M μ B/spAb conjugate was pipetted into the blocked plate and then decanted using the magnetic separator to retain the beads. TFF3 in 100 mM borate (pH 7.5) containing 1 wt% casein was added to the plate and incubated at 23 ± 2 °C with agitation for 5 min. The plate was decanted again and washed 3 times with 100 mM borate (pH 7.5). Finally, the AgNP/2°mpAb/mpAb conjugate was added and the plate was incubated for an additional 5 min using the same conditions. The plate was washed 3 more times with the same washing buffer.

The one-step assay was similar to the stepwise assay, but with the following exceptions. The TFF3 solution and AgNP conjugate were simultaneously added to the plate and incubated with the M μ B conjugate. The TFF3 and AgNP conjugate solutions were concentrated at 2 \times prior to being added in equal volumes to the mixture in the microtiter plate well. For experiments involving human or artificial urine, the stated dilution (if any) of the human or artificial urine was used to prepare the TFF3 solution (1 wt% casein), which was then mixed with an equal volume of AgNP conjugate in 100 mM borate (pH 7.5) with 0.1 wt% casein for a one-step incubation.

For electrochemical detection, the M μ B/spAb-TFF3-mpAb/2°mpAb/AgNP immunocomplex (hereafter, the "immunocomplex") was used without further processing. For spectroscopic

detection, 40 μL of 1 : 2000 SA/HRP : 1 wt% casein in 100 mM borate (pH 7.5) was added to each well and the plate incubated for another 5 min. The plate was then washed 3 more times. 20 μL of 100 mM borate (pH 7.5) were added to each well and the plate agitated for 1 min. 50 μL of TMB substrate solution was added to each well and the reaction was allowed to proceed for 1 min before being quenched with 50 μL of 1.0 M H_2SO_4 . The plate was then immediately read on the plate reader at a wavelength of 450 nm.

Results and discussion

Overview of the *o*Slip design

We recently reported a 3D PAD design that is easily fabricated using the principles of origami (Japanese paper folding).⁶⁰ In the present report we adapted this basic form factor to a TFF3 assay using buffer, artificial urine, and human urine as the matrices. The device design is shown in Scheme 1. It consists of hollow channels³² and a hemichannel,³⁸ which enable microbead flow and faster flow than would be possible in a paper channel,³² and a slip-layer switch,³⁶ which makes it possible to time reagent delivery. Additionally, the design incorporates three screen-printed carbon electrodes for quantitative electrochemical detection, a sample inlet, a sink to drive flow *via* capillary action, dried blue dye, a window to indicate when the sink saturates with fluid, and KMnO_4 , which is dried on the slip layer and used to oxidize the AgNP labels. Two passive forms of amplification are inherent to the detection strategy. One involves a magnet placed behind the working electrode to concentrate M μ Bs, which are part of the assembled immunocomplexes, at the working electrode surface. The other involves the AgNP labels, which provide $\sim 250\,000$ equiv. of electrons per immunocomplex.

Antibody selection, preparation of a AgNP/Ab conjugate, and stepwise detection of TFF3 in a conventional electrochemical cell

To minimize complexity, we attempted to conjugate the mpAbs to the AgNPs by direct physisorption. It is known, however, that not all antibodies retain binding activity towards their target after adsorption onto metal nanoparticles,^{61,62} and indeed we tested eight physisorbed antibodies (Table S1 in the ESI†) and found that only one of them retained activity for TFF3. Accordingly, for the data discussed hereafter, we used an intermediate 2 $^\circ$ Ab for linking the mpAbs to the AgNPs. Specifically, a goat anti-rabbit 2 $^\circ$ Ab was linked to the AgNPs and, after a washing step, the mpAb was bound to the AgNP/2 $^\circ$ mpAb conjugate.

As discussed in the Experimental section, the stepwise electrochemical assay was carried out by first incubating TFF3 with the M μ B/spAb conjugate. After 3 washing steps, the AgNP/2 $^\circ$ mpAb/mpAb conjugate was incubated with the M μ B/spAb-TFF3 composite to form the full immunocomplex. The immunocomplex was then washed 3 times and tested for

detectability in a conventional, three-electrode electrochemical cell.

The results of the foregoing experiments are shown in Fig. 1a, which is a plot of ASV current density as a function of electrode potential for different concentrations of TFF3. The areas under these voltammograms are plotted as a function of the concentration of TFF3 in Fig. 1b. The data reveal a linear region at low TFF3 concentrations followed by a leveling off at higher concentrations. The leveling off is due to saturation of the binding capacity of the spAbs, mpAbs, or both, with TFF3. The low concentration region is expanded in the inset of Fig. 1b, and it shows that the linear part of the TFF3 dose-response curve spans one order of magnitude: 0.010 to 0.100 $\mu\text{g mL}^{-1}$ TFF3, which can be compared to the target range of 0.03–7.0 $\mu\text{g mL}^{-1}$.^{6,12,13} As discussed later, however, further optimization of the assay in the *o*Slip covers a range spanning 2.5 orders of magnitude.

On the basis of these data, we conclude that the conjugation method involving the specific 2 $^\circ$ Ab is effective for linking the mpAb to AgNPs without significantly disrupting the activity of the mpAb toward TFF3. The results also demonstrate the viability of stepwise immunocomplex formation and the electrochemical detection method.

Detection of TFF3 in the *o*Slip

Having shown that the metalloimmunoassay works properly in a conventional electrochemical cell, we now seek to compare those results to the same assay carried out using the paper *o*Slip device. The *o*Slip was prepared for these experiments as follows. First, a 4.0 μL aliquot of 940 μM aqueous KMnO_4 was dried under N_2 on the paper tab of the slip layer (Scheme 1, layer c). The slip layer was then aligned between layers b and d and the device was folded as shown in Scheme 1. A piece of double-sided tape was attached to the top of layer a to hold the *o*Slip in place, and then the folded device was sandwiched between two acrylic plates. The plates were clamped together with two binder clips. Finally, the device was connected to the potentiostat leads and the cylindrical magnet was inserted into a slot in the top acrylic plate just above the working electrode (Fig. S4†).

The immunocomplex was prepared just as it was for the conventional electrochemical cell (stepwise formation), and then it was resuspended in 50.0 μL of 0.10 M PBS buffer (pH 7.4 phosphate buffer containing 0.10 M NaCl). The sample was then injected into the inlet of the *o*Slip. After ~ 15 s, the paper window turned blue, signaling that the 3D channel and sink (Scheme 1) were saturated with solution (approximately the entire 50.0 μL sample) and that flow had therefore stopped. At this cue, the slip layer was pulled until the slip line (Scheme 1) became visible. This positions the paper tab containing the predispensed KMnO_4 directly under the working electrode, resulting in diffusion of MnO_4^- across the 180 μm thickness of the hollow channel and oxidation of the AgNPs immobilized on the M μ Bs and held directly under the working electrode by the magnetic force. Just 12 s was required for complete oxidation of the AgNPs, and then the electrode

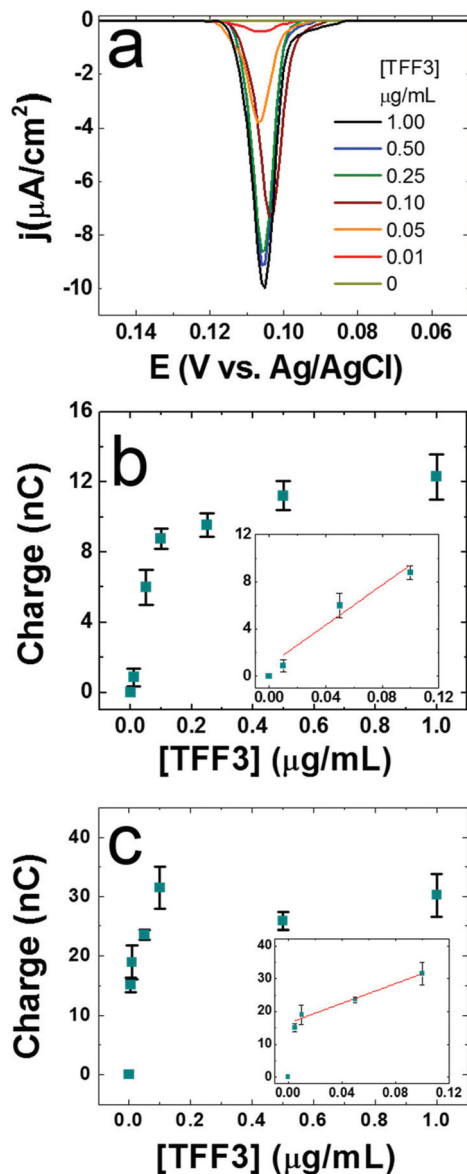


Fig. 1 Electrochemical data for the TFF3 assays carried out in 100 mM borate (pH 7.5) using an immunocomplex prepared by stepwise formation. (a) ASV scans obtained using the conventional electrochemical cell. The linear scan voltammograms started and ended at -0.10 V and 0.40 V (vs. Ag/AgCl), respectively, and the scan rate was 0.050 V s^{-1} . The supporting electrolyte was 67 mM phosphate buffer containing 67 mM NaCl (pH 7.4). The TFF3 concentrations are indicated in the legend. (b) Plot of the charge under the ASVs in (a) as a function of the TFF3 concentration. (c) Plot of the charge under ASVs (not shown) as a function of the TFF3 concentration for assays carried out on the oSlip. The supporting electrolyte was 100 mM phosphate buffer containing 100 mM NaCl (pH 7.4). The following information applies to all results in this figure. The assay reagents were: 20 μ L of 10 μ g mL^{-1} mpAb bound to 0.565 nM AgNPs via 10 μ g mL^{-1} 2° mpAb, 20 μ L of aspirated 10 μ g mL^{-1} spAb bound to 5 mg mL^{-1} M μ Bs, and 20 μ L of TFF3 at the indicated concentrations. The insets indicate the useful dynamic ranges. Each data point represents the mean of 3 replicates and the error bars represent one standard deviation from the mean. Outliers were treated using Dixon's Q test.

potential was stepped to a value that resulted in reduction of Ag^+ for 200 s. Finally, an ASV was obtained and the area under the peak integrated.

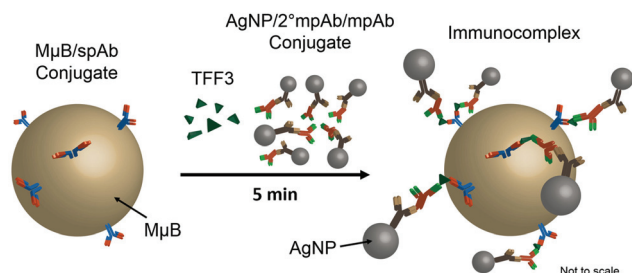
The areas under the ASVs are plotted as a function of the concentration of TFF3 in Fig. 1c. The shape of this plot is similar to that obtained using the conventional cell: a linear region at low TFF3 concentrations followed by a leveling off at higher concentrations. The inset in Fig. 1c expands the linear range for this assay: 0.005 – 0.10 μ g mL^{-1} (recall the target range is 0.03 – 7.0 μ g mL^{-1}).^{6,12,13} Notice that the absolute magnitude of the charge for a particular TFF3 concentration is higher by a factor of two to four in the oSlip compared to the conventional electrochemical cell. We reported this same observation in an earlier preliminary publication that focused on detection of a model complex,⁶⁰ and hence it may be a general finding. The higher signal probably arises from the following factors: magnetic concentration of the AgNPs at the working electrode, a larger working electrode in the oSlip compared to the conventional cell, and confinement of Ag^+ due to the thinness of the paper electrochemical cell.

One important final point: when the TFF3 assay is carried out in the oSlip there is zero background. This is because only AgNPs linked to the M μ Bs *via* TFF3 reside near the working electrode: all other AgNPs pass by the electrode and end up in the sink.

One-step formation and detection of the TFF3 immunocomplex

Our long-term goal is to place all necessary reagents for oSlip immunoassays directly on the sensor. This would simplify its operation, because the user would only have to dispense the sample at the inlet and then pull the slip layer at the designated time. An important first step toward this goal is determining if the TFF3 immunocomplex (M μ B/spAb-TFF3-mpAb/ 2° mpAb/AgNP) can be formed in a single step.

As described in the Experimental section, the one-step immunocomplex was formed by incubating TFF3, the AgNP/ 2° mpAb/mpAb conjugate, and the M μ B/spAb conjugate simultaneously (Scheme 2). After this single step, the immunocomplex was washed 3 times and was then ready for electrochemical detection in the conventional electrochemical cell. The resulting dose–response curve (Fig. 2) reveals a region of increasing charge as the concentration of TFF3 increases until a maximum is reached at ~ 0.10 μ g mL^{-1} , and then the



Scheme 2

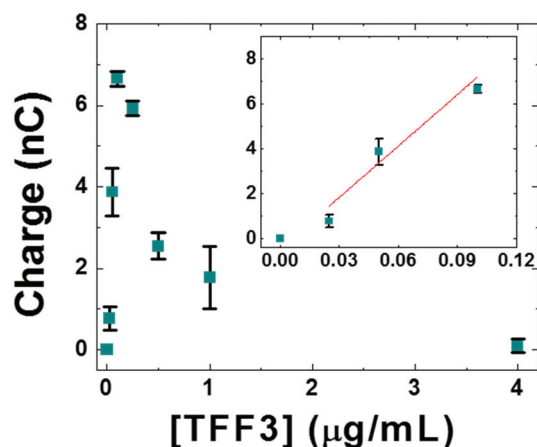


Fig. 2 Plot of the charge under ASVs (not shown) as a function of TFF3 concentration for assays carried out using an immunocomplex prepared by one-step formation. The data were obtained using the conventional electrochemical cell. The immunocomplex was prepared in 100 mM borate (pH 7.5) and with the assay reagents listed in Fig. 1. The supporting electrolyte was 66.7 mM phosphate buffer containing 66.7 mM NaCl (pH 7.4). The inset indicates the useful dynamic range for the dose–response curve. Each data point represents the mean of 3 replicates and the error bars represent the standard deviation of the mean. Outliers were treated using Dixon's *Q* test.

signal decreases. The linear range (Fig. 2, inset) is from 0.025–0.10 $\mu\text{g mL}^{-1}$.

There are some important similarities and differences between the results of the one-step assay, shown in Fig. 2, and the stepwise version of this same experiment (Fig. 1b). The similarities include the linear ranges (compare insets in the two figures) and the magnitudes of the electrochemical signals in the linear range. These observations suggest that there are no fundamental barriers to carrying out formation of the immunocomplex in a single step. The major difference between the two data sets is the shape of the dose–response curves at high TFF3 concentrations. The decrease in signal with increasing TFF3 concentration for the one-step assay is a consequence of the well-known hook effect, which often adversely affects one-step immunoassays when the target is present at high concentration.^{63,64}

The results of the one-step assay are encouraging, but the linear range of the assay (Fig. 2, 0.025–0.10 $\mu\text{g mL}^{-1}$) is not sufficiently coincident with the target range (0.03–7.0 $\mu\text{g mL}^{-1}$) for urinary TFF3.^{6,12,13} In addition, it is important to optimize it for a more realistic matrix than buffer. Accordingly, we focus next on finding conditions that expand the working range of the one-step approach to higher concentrations of TFF3 in artificial urine.

Optimization of one-step incubation in artificial urine

In this section we describe experiments intended to optimize the TFF3 assay so that it covers a broader portion of the target TFF3 concentration range. Artificial urine was selected as the matrix for the optimization process, because it is more similar

to human urine than buffer but not as complex and variable. Furthermore, artificial urine is easier to prepare, handle, and store than human urine.

As a starting point for this study, we used nearly the same experimental conditions described for the one-step assay carried out in buffer. To find optimal conditions for the assay quickly, however, we opted to use a standard ELISA assay (see Experimental section), rather than electrochemistry, to screen through key parameters. Fig. 3a (black data points) shows unoptimized data for the ELISA assay using artificial urine as the matrix and one-step formation of the immunocomplex. The shape of this dose–response curve is similar to that shown in Fig. 2, in that the hook effect is apparent, but the useful dynamic range is more than an order of magnitude broader (0.0005–1.0 $\mu\text{g mL}^{-1}$). This difference can be attributed to one or more of the following factors: the difference in incubation media (artificial urine vs. buffer), the concentration of the M μ B/spAb conjugate (twice as much was used to generate the data in Fig. 3a), and the detection method (ELISA in Fig. 3a and electrochemistry in Fig. 2). The relative contributions of each of these will become apparent later.

To expand the dynamic range of the assay to higher TFF3 concentrations, the binding capacity of the M μ B/spAb conjugate was increased by increasing the concentration of spAb used for reaction with the M μ Bs to 50 $\mu\text{g mL}^{-1}$ (five times higher than was used for the unoptimized data in Fig. 3a). The effect of different concentrations of this more antibody-dense M μ B/spAb conjugate on the assay was then examined. Fig. S1a† is a plot of the ELISA signal as a function of the volume of the M μ B/spAb conjugate (concentration = 5.0 mg mL⁻¹) for a fixed TFF3 concentration of 10.0 $\mu\text{g mL}^{-1}$. This TFF3 concentration was chosen because it is near the upper limit of the target urinary TFF3 concentration range.^{6,12,13} The data in Fig. S1a† reveal a very slight increase in signal as the amount of M μ B/spAb increases, and therefore 80 μL of the M μ B/spAb conjugate was selected as a compromise between cost and performance.

After optimizing the M μ B/spAb conjugate concentration, an ELISA was performed by varying the concentration of TFF3. In this case, the useful dynamic range was shifted from 0.0005–1.0 $\mu\text{g mL}^{-1}$ (Fig. 3a) to 0.05–3.0 $\mu\text{g mL}^{-1}$ TFF3 (Fig. S1b†), which is much more closely matched to the desired range of 0.03–7.0 $\mu\text{g mL}^{-1}$.^{6,12,13}

At this point, we transitioned back to the electrochemical *o*Slip to test these semi-optimized conditions. The results of these experiments (Fig. 3b) are nearly identical to those found by ELISA, including the useful dynamic range of 0.05–3.0 $\mu\text{g mL}^{-1}$ TFF3.

The next step was to try to find assay conditions that further expand the upper end of the dynamic range and reduce the hook effect. Accordingly, we started with the optimized concentration of the M μ B/spAb conjugate and a TFF3 concentration of 5.0 $\mu\text{g mL}^{-1}$ (near the center of the clinical range), and then the concentration of the other half of the antibody sandwich (the AgNP/2^ompAb/mpAb conjugate) was varied. To speed up the screening process, we again resorted

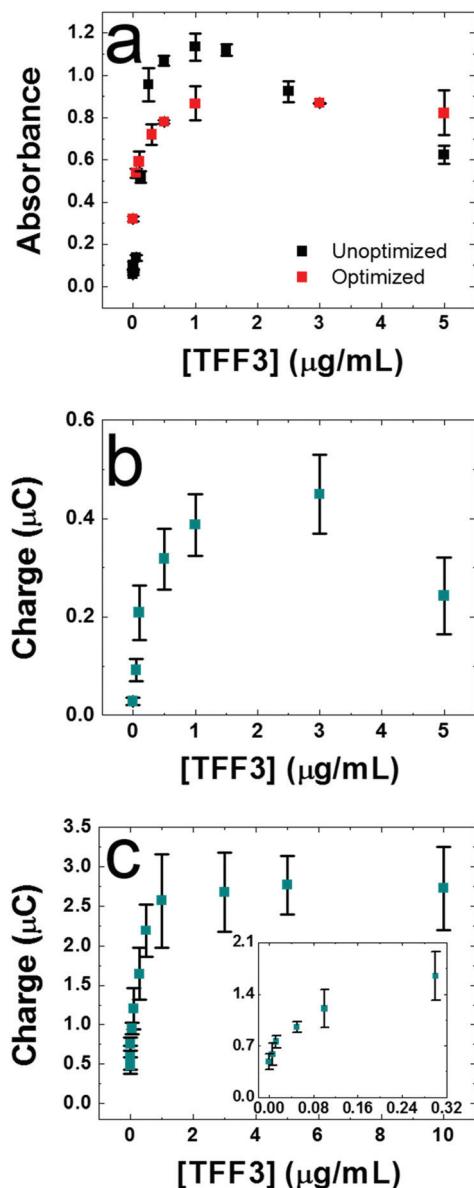


Fig. 3 Optimization of one-step incubation in artificial urine. (a) Unoptimized and optimized TFF3 dose–response curves obtained using spectroscopic detection. Unoptimized assay reagents are the same as the assay reagents listed in Fig. 1 except for the use of 40 μL of 5 mg mL^{-1} $\text{M}\mu\text{B}/\text{spAb}$. Optimized assay reagents are described in (c). (b) Partially optimized TFF3 dose–response curve obtained using electrochemical detection on the *oSlip*. Partially optimized assay reagents are the same as for the unoptimized assay reagents in (a) except for use of 80 μL of $\text{M}\mu\text{B}/\text{spAb}$, 50 $\mu\text{g mL}^{-1}$ spAb , and 5 $\mu\text{g mL}^{-1}$ mpAb . The supporting electrolyte was 100 mM phosphate buffer containing 100 mM NaCl (pH 7.4). (c) Optimized TFF3 dose–response curve obtained using the *oSlip*. Optimized assay reagents are the same as for the partially optimized assay reagents in (b) except for use of 20 μL of 3.39 nM AgNPs. The supporting electrolyte was the same as for (b). The inset indicates the region of the useful dynamic range. The following information applies to all results in this figure: each data point represents the mean of 3–10 replicates and the error bars represent the standard deviation of the mean. Outliers were treated using Dixon's *Q* test.

to ELISA for making these measurements. The results (Fig. S2a†) show that as the $\text{AgNP}/2^\circ\text{mpAb}/\text{mpAb}$ conjugate concentration increases, the ELISA signal also increases. This implies that the binding capacity of the $\text{AgNP}/2^\circ\text{mpAb}/\text{mpAb}$ conjugate, rather than that of the $\text{M}\mu\text{B}/\text{spAb}$ conjugate, limits the dynamic range of the assay.⁶⁴ Accordingly, we selected a $\text{AgNP}/2^\circ\text{mpAb}/\text{mpAb}$ concentration of 3.4 nM as optimal. This value, which is six-fold higher than that used in the earlier experiments, is a compromise between antibody cost and assay performance. Using these optimized conjugate concentrations, we carried out an ELISA as a function of the TFF3 concentration (Fig. S2b†). The dynamic range under these conditions was unchanged at 0.05–3.0 $\mu\text{g mL}^{-1}$, but the hook effect was nearly eliminated. This is apparent in Fig. 3a where the unoptimized and optimized ELISA dose–response curves are compared over a TFF3 concentration range of 0 to 5 $\mu\text{g mL}^{-1}$.

Using these ELISA-optimized conditions, we next obtained a dose–response curve for TFF3 using the *oSlip* (Fig. 3c). The results show that the dynamic range is extended at the low end but not at the high end (0.0125–3.0 $\mu\text{g mL}^{-1}$) compared to the equivalent experiment carried out using the pre-optimized *oSlip* conditions (Fig. 3b). Of course it would be best to expand the range of the sensor to cover the entire relevant clinical range (up to 11 $\mu\text{g mL}^{-1}$), but at least this process eliminated the hook effect and that is a significant accomplishment.

Comparison of the optimized *oSlip* assay to other TFF3 assays

In this section, we discuss figures of merit for the optimized TFF3 assay using the *oSlip* platform and artificial urine as the matrix. The lowest detectable concentration of TFF3, which we define as the lowest concentration of TFF3 for which the standard deviation of the electrochemical signal does not overlap with the standard deviation of the blank, is 0.0125 $\mu\text{g mL}^{-1}$ ($0.75 \pm 0.08 \mu\text{C}$ or $947 \pm 75 \text{ pM}$). On the basis of 10 replicate experiments performed in the absence of TFF3, the limit of blank, defined as the average signal for these 10 replicates, is $0.49 \pm 0.10 \mu\text{C}$. Accordingly, the dynamic range of the optimized assay extends from 0.0125–3.0 $\mu\text{g mL}^{-1}$, spanning almost 2.5 orders of magnitude. The average CV for the data is 17.8%.

A number of TFF3 assays have been reported in the literature,^{1,11,15,65,66} and in Table 1 we compare their figures of merit to those of the *oSlip* assay. While the CVs and limits of detection are more favorable for the previously reported assays, the *oSlip* assay has a comparable or broader dynamic range, requires less than 10 min to perform, requires less steps, is amenable to point-of-care settings, and is much less expensive. Two additional points bear mention. First, the low end of the dynamic range of the other TFF3 assays listed in Table 1 is ~ 1 –3 orders of magnitude lower than the target range of 0.03–7.0 $\mu\text{g mL}^{-1}$,^{6,12,13} and hence it is not very relevant from a biomedical perspective. Second, more careful fabrication and assembly of the *oSlip* would undoubtedly improve the CVs shown in Table 1.

Table 1 Comparison of the TFF3 oSlip assay to literature and commercial TFF3 ELISAs

TFF3 assay type	Lowest detectable concentration ($10^{-3} \mu\text{g mL}^{-1}$)	Dynamic range ^f ($10^{-3} \mu\text{g mL}^{-1}$)	Intra-assay CV	Total assay time (min)
oSlip	12.5	12.5–3000	17.8%	10
Literature ELISA ^a	0.040	0.040–1.32	1.8–3.2%	100
Validation of commercial ELISA ^b	0.25	0.25–2	3.6–6.4%	—
Literature ELISA ^c	0.78	0.78–100	6.0%	—
Literature ELISA ^d	5	5–1250	1.6–4.2%	310
Commercial ELISA ^e	0.039	0.039–2.5	1.1–2.2%	270

^a A literature ELISA using two rabbit polyclonal antibodies.¹ ^b Testing performed on a commercial (Biovendor) TFF3 ELISA based on two polyclonal antibodies.¹⁵ ^c A literature ELISA using a mouse monoclonal antibody and a rabbit polyclonal antibody.¹¹ ^d A literature ELISA using two mouse monoclonal antibodies.⁶⁶ ^e A commercial ELISA kit from R & D Systems based on a monoclonal antibody and a polyclonal antibody.⁶⁵ ^f The target range is 0.03–7.0 $\mu\text{g mL}^{-1}$.^{6,12,13}

To further benchmark the oSlip assay, we performed a side-by-side comparison of its performance against results from a commercial TFF3 ELISA kit obtained from R & D Systems.⁶⁵ To directly compare the assays, we spiked known TFF3 concentrations into artificial and human urine (tested beforehand to ensure negligible intrinsic TFF3 concentrations; see Table S2 in the ESI†). The results of each assay were then compared to one another and to the known TFF3 concentrations.

To select appropriate conditions for the comparison, we had to consider the capabilities of each assay. For instance, the dynamic range for the R & D Systems assay is reported to be 39.0–2500 pg mL^{-1} and for the oSlip assay it is 0.0125–3.0 $\mu\text{g mL}^{-1}$. Additionally, the R & D Systems assay reports a near-zero-signal for concentrated artificial or human urine samples containing 2500 pg mL^{-1} of TFF3, which is the upper end of the linear range of the assay (data not shown). As a result, for the R & D Systems assay, we spiked known TFF3 concentrations into artificial or human urine and then diluted the mixture by a factor of 500 using the buffer provided with the kit (*i.e.*, the concentration of artificial urine is very low).⁶⁵ To match the assays as closely as possible, we also diluted artificial and human urine by a factor of 500 using 100 mM borate (pH 7.5) for the oSlip assay.

The TFF3 samples used with the R & D Systems assay were compared to a calibration curve (Fig. S3†) generated by following the kit protocol.⁶⁵ The TFF3 samples used for the oSlip assay were compared to a calibration curve generated in 100 mM borate (pH 7.5) using the optimized conditions in Fig. 3c. Fig. 4a shows the calibration curve for the oSlip, and Fig. 4b provides an expanded view of Fig. 4a at the low end of the TFF3 concentration range. An equation was fitted to the calibration curve (over the range 0.00313–0.50 $\mu\text{g mL}^{-1}$) based on the SGompertz dose–response function, and this function was then used to determine the TFF3 concentrations in the spiked samples.

Table 2 compares the spiked TFF3 concentrations determined by the R & D Systems and oSlip assays. The percent relative errors for samples compared between the two assays (column 5) are $\leq 15\%$, demonstrating good agreement. However, the percent relative errors that compare the known (spiked) TFF3 concentrations to those determined by the two

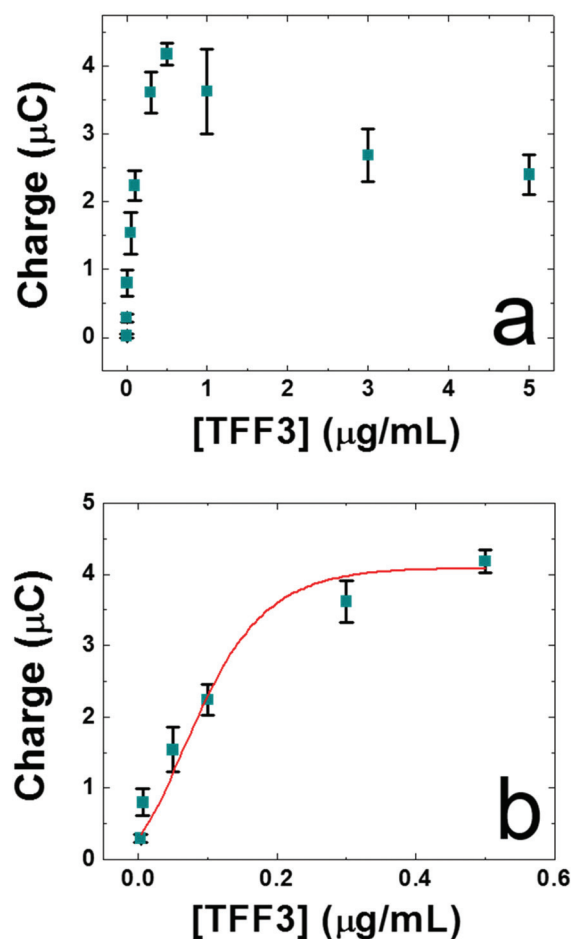


Fig. 4 (a) TFF3 dose–response curve obtained by carrying out sandwich formation in one step using 100 mM borate (pH 7.5) and using the optimized assay reagent conditions described for Fig. 3c. Electrochemical detection was performed on the oSlip. The supporting electrolyte was 100 mM phosphate buffer containing 100 mM NaCl (pH 7.4). Each data point represents the mean of 6 replicates and the error bars represent the standard deviation of the mean. Outliers were treated using Dixon's Q test. (b) An expanded view of the low-concentration range of the curve in (a). The data were fitted to the SGompertz dose–response function in OriginPro 8.

Table 2 Evaluation of TFF3 samples spiked in dilute artificial urine and dilute human urine matrices using the optimized oSlip assay and a commercial TFF3 ELISA kit

Column	1	2	3	4	5	6	7
Sample	Spiked TFF3 concentration ($\mu\text{g mL}^{-1}$)	TFF3 concentration determined from oSlip assay ($\mu\text{g mL}^{-1}$)	TFF3 concentration determined from commercial assay ^a ($\mu\text{g mL}^{-1}$)	% Relative error between oSlip assay result and commercial assay result	% Relative error between oSlip assay result and spiked TFF3 concentration	% Relative error between commercial assay result and spiked TFF3 concentration	
Artificial urine	0.20	0.11 ± 0.03	—	—	44	—	
	0.040	0.049 ± 0.024	0.043 ± 0.007	15	24	8	
	0.0050	0.0049 ± 0.0200	0.0054 ± 0.0024	10	3	8	
Human urine sample 1	0.20	0.13 ± 0.05	—	—	36	—	
	0.040	0.059 ± 0.025	0.060 ± 0.018	1	48	50	
Human urine sample 2	0.20	0.092 ± 0.030	—	—	54	—	
	0.040	0.066 ± 0.026	0.058 ± 0.015	15	66	44	

^a R & D Systems.

assays spanned a much broader range of values for both assays (Table 2, columns 6 and 7). At least in human urine samples, the level of accuracy of the two assays is indistinguishable. The underlying reason for the surprisingly large errors in both assays requires additional investigation. Clearly, however, as a lab scale prototype there is still much room for improving the oSlip assay, but it is reasonable to expect better assay performance from the R & D Systems assay which has been available commercially for many years.

Summary and conclusions

In summary, we have developed a quantitative metalloimmunoassay that can determine TFF3 concentrations in human urine with an accuracy equivalent to a commercial kit. The oSlip assay is fast relative to the R & D systems assay (<10 min compared to 270 min), and it is very simple to carry out. The oSlip assay is sufficiently sensitive to detect TFF3 concentrations at the low end of the target TFF3 concentration range ($0.03\text{--}7.0 \mu\text{g mL}^{-1}$).^{6,12,13} The oSlip assay has a dynamic range of ~ 2.5 orders of magnitude, but in its current form is not able to determine TFF3 concentrations at the high end of the clinical range. Additional significant advantages of the approach used in the oSlip are that it requires only a single incubation step, employs environmentally stable metal NP labels instead of more labile enzyme labels, and is compatible with an inexpensive, manufacturable paper detection platform.

Despite the many positive aspects of the TFF3 oSlip assay, problems remain. First, its current configuration does not support measurement at the high end of the target range of TFF3 concentrations. The high end of the urinary TFF3 range is important, because results in this part of the range correlate with the presence of CKD.^{6,11,12} While the oSlip assay can indicate that the level of urinary TFF3 is abnormally high, without quantitation up to the highest level of the target range, likeli-

hood of CKD cannot be precisely determined. Second, the accuracy of oSlip-based detection of TFF3 in spiked samples needs improvement. We believe that our recently developed NoSlip device, which eliminates the slip layer, is easier to fabricate reproducibly, and provides a better means for oxidation of the AgNP labels will, at least in part, be able to address these problems.⁶⁷ The results of those experiments will be reported in due course.

Acknowledgements

We gratefully acknowledge financial support from Novartis and the National Science Foundation (Grant No. CBET-1402242). We also thank the Robert A. Welch Foundation (Grant F-0032) for sustained research support. We also acknowledge helpful discussions with Dr. Susan Bromley (Novartis).

References

- 1 E. M. Vestergaard, S. S. Poulsen, H. Grønbaek, R. Larsen, A. M. Nielsen, K. Ejlskjær, J. T. Clausen, L. Thim and E. Nexø, *Clin. Chem.*, 2002, **48**, 1689–1695.
- 2 W. Hoffmann, *Cell. Mol. Life Sci.*, 2005, **62**, 2932–2938.
- 3 J. V. Bonventre, V. S. Vaidya, R. Schmouder, P. Feig and F. Dieterle, *Nat. Biotechnol.*, 2010, **28**, 436–440.
- 4 R. G. Fassett, S. K. Venuthurupalli, G. C. Gobe, J. S. Coombes, M. A. Cooper and W. E. Hoy, *Kidney Int.*, 2011, **80**, 806–821.
- 5 T. C. Fuchs and P. Hewitt, *AAPS J.*, 2011, **13**, 615–631.
- 6 B. C. Astor, A. Köttgen, S.-J. Hwang, N. Bhavsar, C. S. Fox and J. Coresh, *Am. J. Nephrol.*, 2011, **34**, 291–297.
- 7 Y. Yu, H. Jin, D. Holder, J. S. Ozer, S. Villarreal, P. Shughrue, S. Shi, D. J. Figueroa, H. Clouse, M. Su, N. Muniappa, S. P. Troth, W. Bailey, J. Seng,

- A. G. Aslamkhan, D. Thudium, F. D. Sistare and D. L. Gerhold, *Nat. Biotechnol.*, 2010, **28**, 470–477.
- 8 J. Coresh, B. C. Astor, T. Greene, G. Eknayan and A. S. Levey, *Am. J. Kidney Dis.*, 2003, **41**, 1–12.
- 9 V.-C. Wu, C.-H. Wu, T.-M. Huang, C.-Y. Wang, C.-F. Lai, C.-C. Shiao, C.-H. Chang, S.-L. Lin, Y.-Y. Chen, Y.-M. Chen, T.-S. Chu, W.-C. Chiang, K.-D. Wu, P.-R. Tsai, L. Chen, W.-J. Ko and for the NSARF Group, *J. Am. Soc. Nephrol.*, 2014, **25**, 595–605.
- 10 P. Devarajan, *Cancer Ther.*, 2005, **3**, 477–488.
- 11 T. Du, H. Luo, H. Qin, F. Wang, Q. Wang, Y. Xiang and Y. Zhang, *PLoS One*, 2013, **8**, e80271.
- 12 D. Lebherz-Eichinger, B. Tudor, H. J. Ankersmit, T. Reiter, M. Haas, F. Roth-Walter, C. G. Krenn and G. A. Roth, *PLoS One*, 2015, **10**, e0138312.
- 13 D. Brott, S. Adler, R. Arani, S. Lovick, M. Pinches and S. Furlong, *Drug Des., Dev. Ther.*, 2014, 227.
- 14 M. H. Samson, P. Chaiyarit, H. Nortvig, E. M. Vestergaard, E. Ernst and E. Nexø, *Clin. Chem. Lab. Med.*, 2011, **49**, 861–868.
- 15 M. H. Samson and E. Nexø, *Clin. Chem. Lab. Med.*, 2011, **49**, 2057–2060.
- 16 D. Mabey, R. W. Peeling, A. Ustianowski and M. D. Perkins, *Nat. Rev. Microbiol.*, 2004, **2**, 231–240.
- 17 A. J. Tüdös, G. A. J. Besselink and R. B. M. Schasfoort, *Lab Chip*, 2001, **1**, 83–95.
- 18 P. Connolly, *Biosens. Bioelectron.*, 1995, **10**, 1–6.
- 19 S. A. Sundberg, A. Chow, T. Nikiforov and H. G. Wada, *Drug Discovery Today*, 2000, **5**, 92–103.
- 20 P. Lisowski and P. K. Zarzycki, *Chromatographia*, 2013, **76**, 1201–1214.
- 21 L. Kang, *Drug Discovery Today*, 2008, **13**, 1–13.
- 22 J. Wölcke and D. Ullmann, *Drug Discovery Today*, 2001, **6**, 637–646.
- 23 Y.-H. Chen, Z.-K. Kuo and C.-M. Cheng, *Trends Biotechnol.*, 2015, **33**, 4–9.
- 24 G. M. Chertow, *J. Am. Soc. Nephrol.*, 2005, **16**, 3365–3370.
- 25 A. W. Martinez, S. T. Phillips, M. J. Butte and G. M. Whitesides, *Angew. Chem., Int. Ed.*, 2007, **46**, 1318–1320.
- 26 H. Liu and R. M. Crooks, *J. Am. Chem. Soc.*, 2011, **133**, 17564–17566.
- 27 C. K. W. Koo, F. He and S. R. Nugen, *Analyst*, 2013, **138**, 4998–5004.
- 28 W. Dungchai, O. Chailapakul and C. S. Henry, *Anal. Chem.*, 2009, **81**, 5821–5826.
- 29 H. Noh and S. T. Phillips, *Anal. Chem.*, 2010, **82**, 8071–8078.
- 30 G. E. Fridley, H. Le and P. Yager, *Anal. Chem.*, 2014, **86**, 6447–6453.
- 31 Y. Koo, J. Sankar and Y. Yun, *Biomicrofluidics*, 2014, **8**, 054104.
- 32 C. Renault, X. Li, S. E. Fosdick and R. M. Crooks, *Anal. Chem.*, 2013, **85**, 7976–7979.
- 33 X. Yang, O. Forouzan, T. P. Brown and S. S. Shevkoplyas, *Lab Chip*, 2012, **12**, 274–280.
- 34 J. L. Osborn, B. Lutz, E. Fu, P. Kauffman, D. Y. Stevens and P. Yager, *Lab Chip*, 2010, **10**, 2659–2665.
- 35 X. Liu, M. Mwangi, X. Li, M. O'Brien and G. M. Whitesides, *Lab Chip*, 2011, **11**, 2189–2196.
- 36 H. Liu, X. Li and R. M. Crooks, *Anal. Chem.*, 2013, **85**, 4263–4267.
- 37 L. Ge, P. Wang, S. Ge, N. Li, J. Yu, M. Yan and J. Huang, *Anal. Chem.*, 2013, **85**, 3961–3970.
- 38 C. Renault, J. Koehne, A. J. Ricco and R. M. Crooks, *Langmuir*, 2014, **30**, 7030–7036.
- 39 G. M. Whitesides, *Lab Chip*, 2013, **13**, 4004–4005.
- 40 S. Ge, L. Ge, M. Yan, X. Song, J. Yu and J. Huang, *Chem. Commun.*, 2012, **48**, 9397–9399.
- 41 A. Apilux, Y. Ukita, M. Chikae, O. Chailapakul and Y. Takamura, *Lab Chip*, 2013, **13**, 126–135.
- 42 G. E. Fridley, H. Le and P. Yager, *Anal. Chem.*, 2014, **86**, 6447–6453.
- 43 C.-M. Cheng, A. W. Martinez, J. Gong, C. R. Mace, S. T. Phillips, E. Carrilho, K. A. Mirica and G. M. Whitesides, *Angew. Chem., Int. Ed.*, 2010, **49**, 4771–4774.
- 44 Y. Wu, P. Xue, Y. Kang and K. M. Hui, *Anal. Chem.*, 2013, **85**, 8661–8668.
- 45 A. C. Araújo, Y. Song, J. Lundeberg, P. L. Ståhl and H. Brumer, *Anal. Chem.*, 2012, **84**, 3311–3317.
- 46 D. P. Kalogianni, L. M. Boutsika, P. G. Kouremenou, T. K. Christopoulos and P. C. Ioannou, *Anal. Bioanal. Chem.*, 2011, **400**, 1145–1152.
- 47 P. B. Allen, S. A. Arshad, B. Li, X. Chen and A. D. Ellington, *Lab Chip*, 2012, **12**, 2951–2958.
- 48 K. Scida, B. Li, A. D. Ellington and R. M. Crooks, *Anal. Chem.*, 2013, **85**, 9713–9720.
- 49 J. Lu, S. Ge, L. Ge, M. Yan and J. Yu, *Electrochim. Acta*, 2012, **80**, 334–341.
- 50 Y. Wang, L. Ge, P. Wang, M. Yan, S. Ge, N. Li, J. Yu and J. Huang, *Lab Chip*, 2013, **13**, 3945–3955.
- 51 H. Liu, Y. Xiang, Y. Lu and R. M. Crooks, *Angew. Chem., Int. Ed.*, 2012, **51**, 6925–6928.
- 52 G.-H. Chen, W.-Y. Chen, Y.-C. Yen, C.-W. Wang, H.-T. Chang and C.-F. Chen, *Anal. Chem.*, 2014, **86**, 6843–6849.
- 53 J. C. Cunningham, N. J. Brenes and R. M. Crooks, *Anal. Chem.*, 2014, **86**, 6166–6170.
- 54 P. B. Allen, S. A. Arshad, B. Li, X. Chen and A. D. Ellington, *Lab Chip*, 2012, **12**, 2951–2958.
- 55 B. A. Rohrman and R. R. Richards-Kortum, *Lab. Chip*, 2012, **12**, 3082–3088.
- 56 D. M. Cate, J. A. Adkins, J. Mettakoonpitak and C. S. Henry, *Anal. Chem.*, 2015, **87**, 19–41.
- 57 D. D. Liana, B. Raguse, J. J. Gooding and E. Chow, *Sensors*, 2012, **12**, 11505–11526.
- 58 C. Parolo and A. Merkoçi, *Chem. Soc. Rev.*, 2013, **42**, 450–457.
- 59 A. K. Yetisen, M. S. Akram and C. R. Lowe, *Lab Chip*, 2013, **13**, 2210–2251.
- 60 K. Scida, J. C. Cunningham, C. Renault, I. Richards and R. M. Crooks, *Anal. Chem.*, 2014, **86**, 6501–6507.

- 61 S. V. Sule, M. Sukumar, W. F. Weiss, A. M. Marcelino-Cruz, T. Sample and P. M. Tessier, *Biophys. J.*, 2011, **101**, 1749–1757.
- 62 D. D. D. Ma, *Science*, 2003, **299**, 1874–1877.
- 63 J. O. Utgaard, J. Frengen, T. Stigbrand, A. Ullen, R. Schmid and T. Lindmo, *Clin. Chem.*, 1996, **42**, 1702–1708.
- 64 S. Amarasiri Fernando and G. S. Wilson, *J. Immunol. Methods*, 1992, **151**, 47–66.
- 65 R & D Systems Quatikine TFF3 ELISA Kit.
- 66 E. Bignotti, A. Ravaggi, R. A. Tassi, S. Calza, E. Rossi, M. Falchetti, C. Romani, E. Bandiera, F. E. Odicino, S. Pecorelli and A. D. Santin, *Br. J. Cancer*, 2008, **99**, 768–773.
- 67 J. C. Cunningham, M. R. Kogan, Y.-J. Tsai, L. Luo, I. Richards and R. M. Crooks, *ACS Sens.*, 2016, **1**, 40–47.